Evaluating methane emission quantification performance and uncertainty of aerial technologies via high-volume single-blind controlled releases

Jeffrey Rutherford[1,a], Evan Sherwin[1], Yulia Chen[1], Sam Aminfard[2], Adam R. Brandt[1*]

[1] Department of Energy Resources Engineering, Stanford University.
[2] ExxonMobil Upstream Research Company
*Corresponding author: abrandt@stanford.edu
[a] Present affiliation: Highwood Emissions Management

This is a non-peer reviewed preprint submitted to EarthArXiv. This paper is being submitted to *Environmental Science & Technology* for peer review.

Abstract

Methane (CH_4) from oil and gas (O&G) activities is a known contributor to global anthropogenic methane emissions and recent research has demonstrated that a small fraction of large emitters contribute to the majority of total emissions. In this study, we perform a single-blind evaluation of the quantification capabilities of three airplane-based technologies (Bridger Photonics' Gas Mapping LiDAR, Carbon Mapper's Global Airborne Observatory, and GHGSat-AV) with a focus on large emitters (10-2,000+ kg h^{-1} CH_4). In two 2021 campaigns, metered natural gas was released concurrently with overpasses by the tested technologies. Results were submitted by operators in a three-stage unblinding process. All teams detected 100% of releases above 50 kg h^{-1} CH_4. The teams report parity slopes of 0.35 to 1.06, with R^2 values of 0.35 to 0.78. After 10-meter anemometer wind measurements were unblinded, two out of three teams significantly reduced variance in the parity slope, highlighting the importance of accurate wind data. After half of metered release volumes were subsequently unblinded, improvement was mixed. These results suggest that multiple commercially available technologies can reliably detect larger point-source methane emissions, with varying quantification performance and trade-offs between survey area coverage and instrument sensitivity.

Introduction

The global oil and gas (O&G) industry is estimated to account for an estimated 30% of global anthropogenic emissions of methane (CH_4), a powerful greenhouse gas (GHG) [1]. Early analysis by Brandt et al. [2] found that CH_4 emissions follow extreme distributions, whereby approximately 5% of sources account for greater than 50% of total emissions. Recent field campaigns find numerous point source emissions exceeding 1 tonne CH_4 per hour [3]–[8], an order of magnitude greater than any point source identified in previous ground-based campaigns at oil and gas production facilities [9]. Because of these extreme distributions, a small number of large emissions sources can cause a large fraction overall emissions. While this is beneficial in some ways, it makes detection more challenging due to the dispersed and intermittent nature of uncommon large emissions spread across a large infrastructure.

Given this new understanding of emission size distributions, regulators and technology developers are re-evaluating leak detection and repair (LDAR) technologies and protocols. Traditional LDAR programs approved by regulators and adopted by companies have typically used Environmental Protection Agency (EPA) Method 21 and optical gas imaging (OGI) infrared cameras. These approaches have demonstrated success in reducing CH_4 emissions over years [10]. However, these ground-based surveys are cost- and time- intensive, which limits the scalability of surveys [11]. In addition, large emitters are likely to originate from tanks, unlit flares, and pipelines, sources which can be difficult to access from the ground [12], [13]. Compared to traditional, ground-based approaches, aerial surveys cover significantly more upstream facilities on a daily basis (in some cases >1000 sites/d), and thus may be better suited to identifying emitters at high magnitudes.

Many airborne methane sensing technologies have performed controlled release testing [14]–[16]. However, only some of these tests use a blind study design (single or double), many studies have sample sizes below 10 measurements, and only one has tested metered releases above 100 kg h^{-1} CH_4 [17]. The 2018 Stanford-Environmental Defense Fund Methane Monitoring Challenge (MMC) is a recent example of a single-blind trial, but at relatively low controlled release rates [18]. In October 2019, Sherwin, Chen, et al. led what is the first peer-reviewed single blind controlled release field trial of an airborne CH_4 detection and quantification technology with metered values above kg h^{-1} CH_4, with releases ranging from 20 to >1,000 kg h^{-1} CH_4. That study evaluated the Kairos Aerospace system, collecting > 200 single-blind aerial measurements [17]. Testing additional technologies at higher-end release volumes in the range of 100-2,000+ kg h^{-1} CH_4 is needed to improve our understanding of quantification performance at these large emissions sizes, observed frequently in the field [3], [19], [20].

Understanding the quantification uncertainty and potential biases of aerial detection is essential to establish confidence and correctly interpret results of these emerging technologies. In this study, we conduct a single-blind controlled release experiment of the high-volume, point-source quantification capabilities of three aerial technologies: Bridger Photonics Gas Mapping LiDAR (GML), Carbon Mapper Global Atmospheric Observatory (GAO), and GHGSat-AV. This focus on quantification uncertainty of point-source emitters is distinct from studies which assess detection capabilities near the minimum detection limits of aerial technologies [21], [22]. We do

assess quantification at low flow rates, however additional data points and in some cases a wider range of volumes would be required to rigorously assess a technology's minimum detection limit, as in Bell et al. [23]. For consistency with previous studies, we follow experimental protocols of the Sherwin, Chen et al. [17] assessment of Kairos Aerospace and the single-blind testing protocols of the Methane Emissions Technology Evaluation Center [24]. Experiments were conducted in two separate campaigns in Gardendale, TX (July-August, 2021) and Ehrenberg, AZ (October-November, 2021).

We employ a novel staged unblinding process to gain additional insight. After submitting fully blind estimates, participants could resubmit emission estimates after being provided ground-based wind measurements (Stage 2 unblinding). This provides additional insight into the uncertainty introduced into measurements from the simulated wind speed estimates commonly used in the field. Afterward, participants were lastly given actual metered values for approximately half of the release volumes (Stage 3 unblinding) and could update or tune their algorithms for local conditions before submitting a final round of estimates for the remaining blind releases. This third stage of unblinding allows teams to tune their methods based on performance on the unblinded data and test accuracy of these changes using the remaining blinded data.

Methods

Description of technologies

Three separate aerial technologies were tested in this study. The major focus of the testing was on quantification accuracy for a large number of plumes including some with very large emissions rates. Very few measurements were allocated to small release volumes where true-false detection becomes an issue. The GHGSat and Carbon Mapper technologies are based on passive infrared spectroscopy, where the spectrometer (sensitive to short-wave infrared bands) receives solar electromagnetic radiation reflected from Earth. The GHGSat-AV technology is a compact, aircraft-adapted design based on the same concept as the GHGSat constellation of microsatellites, which detect point source emitters using hyperspectral imaging spectrometers [25]. Carbon Mapper operates two similar spectrometer instruments on separate aircraft, which have been the basis of numerous published scientific studies [5], [8] and peer reviewed controlled release testing up to 100 kg h^{-1} CH_4 [16]. This study tests Carbon Mapper using the Global Airborne Observatory (GAO) aircraft. In contrast, the Bridger Photonics (henceforth Bridger) technology is based on active infrared spectroscopy. The Gas Mapping LiDAR (GML) unit contains a laser which sends and receives a beam of radiation in a portion of the spectrum in which methane is active. Spectroscopy measurements are performed on the received radiation to determine path-integrated methane concentration [26]. Peer reviewed controlled release testing of the Bridger GML technology have been published for emission rates up to 22 kg h^{-1} CH_4 [21]. Internal testing has also been published for emission rates up to 550 kg h^{-1} CH_4[27]. Note that the data that forms the basis of this study was also analyzed by Bell et al. [23].

An important differentiator between platforms is flight altitude. Carbon Mapper and GHGSat-AV performed testing at altitudes ~ 9,000-10,000 feet above ground level (agl) most days (GHGSat-AV's average flight altitude on October 21 was 6,572 feet agl), while Bridger

performed testing at ~690 feet agl. Additional technical specifications of the three aerial technologies are provided in **Table S1** and **Table S3**.

Test location and setup

Controlled release testing took place in two rounds. First, in August in Gardendale, Texas (TX) and second in October-November near Ehrenberg, Arizona (AZ). We selected release locations based on ground conditions, distance from urban environments and potential confounding methane sources, and convenience for methane sensing technology operators.

Photos and a schematic of the release system located in a cleared field of an industrial park in Midland, TX are given in Rutherford et al. [28] (see Figures 1-7 in [28]). Gas was supplied by two compressed natural gas (CNG) tube trailers, each with rated capacity of 120 thousand standard cubic feet (mscf) and working capacity of 100 mscf. Trailer pressures varied from ~2,500 to ~500 pounds per square inch gauge (psig) depending on remaining gas levels. One Tescom pressure regulator per CNG trailer was used to manually control flow levels and step down gas pressure from the trailer output pressure to 250 psig. To reduce cooling of the regulators, a catalytic heater partially compensated for Joule-Thomson cooling. Gas was transported to two release stacks via three 25 feet long, 1-inch rubber hoses. The first release stack was 2-inch diameter stainless steel. The second release stack was 4-inch diameter carbon steel. Metering was performed with two Sierra Instruments QuadraTherm 640i meters placed close to the release stack (IDs: 162928 and 218645, see Rutherford et al. [28] for characteristics).

Photos and a schematic of the release system located in open desert near Ehrenberg, AZ are given in Rutherford et al. [28] (see Figures 8-15 in [28]) . Gas was supplied by a liquefied natural gas (LNG) trailer with rated capacity of 892.3 mscf and working capacity of 800 mscf. The trailer was generally filled to 150 psig with gas at the boiling point of LNG, -162 ºC. A separate heater trailer, equipped with boilers and a glycol heat exchanger was used to vaporize the LNG to 20-25 ºC from its baseline temperature of ~ -160 °C. After reheating and pressure regulation, gas is transported to the release trailer through an 8-inch hose. The metering and release trailer in Ehrenberg consisted of four parallel pipes of size 0.5-inch, 2-inch, 4-inch, and 8-inch carbon steel pipe. On the 0.5 inch pipe, metering was performed with a Micro Motion ELITE Coriolis meter (ID 21175085). On the remaining three, larger pipes, metering was performed with a Sierra Instruments Quadratherm 640i meter (ID 218645 during GHGSat-AV testing and ID 308188 during Bridger testing, see Rutherford et al. [28] (see Table 11 in [28]). For redundancy, data were recorded via three separate streams (in order of decreasing priority): (i) a Eurotherm Nanodac automatic data logger, (ii) a Zoom live stream of the meters (digitized when needed using Optical Character Recognition), and (iii) real-time hand-recording of instantaneous rate when the aircraft was directly overhead. Given that data was logged at different frequencies (Nanodac = secondly, Texas optical character recognition = 10 secondly (due to low quality caused by sun glare), Arizona optical character recognition = secondly, real-time field data recorded at revisit intervals) data loss did occur in a small number of cases, with minimal effect on our results.

Survey protocol

For each day of testing, an aerial technology conducted repeated measurements of the methane point source operated by Stanford over continuous periods of time. Each technology flight path approximated a "figure-8" pattern, and revisit times were, on average, 4.1 minutes for Bridger, 2.1 minutes for Carbon Mapper, and 4.1 minutes for GHGSat-AV (see **Table S3** for a summary of daily start times, durations, revisit times, altitude flown, and average wind speed for each team).

Release schedules were tentatively designed ahead of time to approximate the heavy-tailed distributions observed in the field, e.g. in Chen, Sherwin et al. [3]. Emphasis (~ 50% share) was given to flow rates of 50-500 kg h^{-1} CH_4. Flow rates < 50 kg h^{-1} CH_4 are outside the 100% detection range for the passive airplane technologies tested here, and thus outside the main focus of this paper. Flow rates > 500 kg h^{-1} CH_4 were released sparingly due to the high cost of such tests. Flow rates > 1000 kg h^{-1} CH_4 most commonly coincided with satellite overpasses to maximize efficient use of gas[29].

In order to ensure sufficient plume development time, the flow rate was not changed at every overpass. On average, the flow rate was changed every 5 overpasses during the Bridger trials (range of 1-8), every 6 overpasses during the Carbon Mapper trials (range of 1-18), and every 4 overpasses during the GHGSat-AV trials (range of 1-12).

The survey protocol, based on the Advancing Development of Emissions Detection protocol[24], is summarized in more detail in a standardized reporting document designed in collaboration with Colorado State University (see additional description in Rutherford et al. [28]). In addition to following the survey protocol, operators were asked to acquire measurements using a protocol mimicking field operations as closely as possible. Prior to the controlled release experiments, participants were expected to provide a detailed description of the methodology employed during the surveys.

Following completion of the testing, results were reported in three rounds in a "staged unblinding" process:

- Stage 1 (fully blinded): Results were reported by teams using their standard field protocol (i.e., no additional on-the-ground data was provided by Stanford).
- Stage 2 (unblinded wind): Once fully blinded estimates were received from all teams, we conducted the first "unblinding", and all teams were given a one-month opportunity to recompute emission estimates after being given measured in situ 10-m wind speeds and directions (as recorded onsite with an ultrasonic anemometer) and the precise coordinates of the release point.
- Stage 3 (partially unblinded emission rates): Once stage 2 estimates were received from all teams there was an additional unblinding of approximately half of the gas release dataset which the teams could use to tune algorithms and re-estimate the remaining blind data points. The final deadline for stage 3 was February 28, 2022.

After the final deadline, Stanford released the actual methane volumes and additional documentation surrounding the release to teams (see **Table S5** for a timetable of when estimates were received from teams by Stanford at each stage).

Data processing

The operator data reporting sheets and Stanford logged data were loaded into a Python script for data processing and results generation. The data processing script consists of: (i) loading and averaging time series of Stanford release volumes and wind data, (ii) merging by matching timestamps with operator reported datasets, and (iii) selectively excluding overpasses based on Stanford quality control criteria, and (iv) uncertainty quantification. Data exclusion criteria are summarized in Rutherford et al. [28]. Note that uncertainty in actual release rates by Stanford are reported to match the uncertainties reported by participating teams. GHGSat-AV and Carbon Mapper both reported uncertainty as 1-sigma. Bridger does not provide uncertainty estimates commercially.

To accurately understand uncertainty of the QuadraTherm 640i flow meter in field conditions, a set of experiments was performed on October 29th – October 31st. 18 intercomparison tests were performed where various sets of two out of the three Stanford QuadraTherm meters were installed in series such that all gas flowing through the first meter flowed through the second meter. By sequentially commanding different flow levels we are able to approximately characterize the (i) short term noise and (ii) long term bias which may result from mal-installation of the QuadraTherm meter (which is possible even if the meter is installed carefully). These resulting uncertainties are incorporated into measured volumes via our characterization of meter uncertainty via simulation with 10,000 Monte Carlo realizations, described in Rutherford et al. [28].

We report quantification performance, similarly to Ravikumar et al. [18] and Sherwin, Chen et al. [17], as a linear fit between actual and reported emission rates using ordinary least squares linear regression.

Results and Discussion

Figure 1 shows plume false color imagery for Bridger, Carbon Mapper, and GHGSat-AV. Spectroscopy data collected by the teams are used to generate two-dimensional imagery of the methane concentration enhancements in the detected plume. This information about the gas plume, in combination with other data such as wind speed estimates, is used to infer the emission rate.

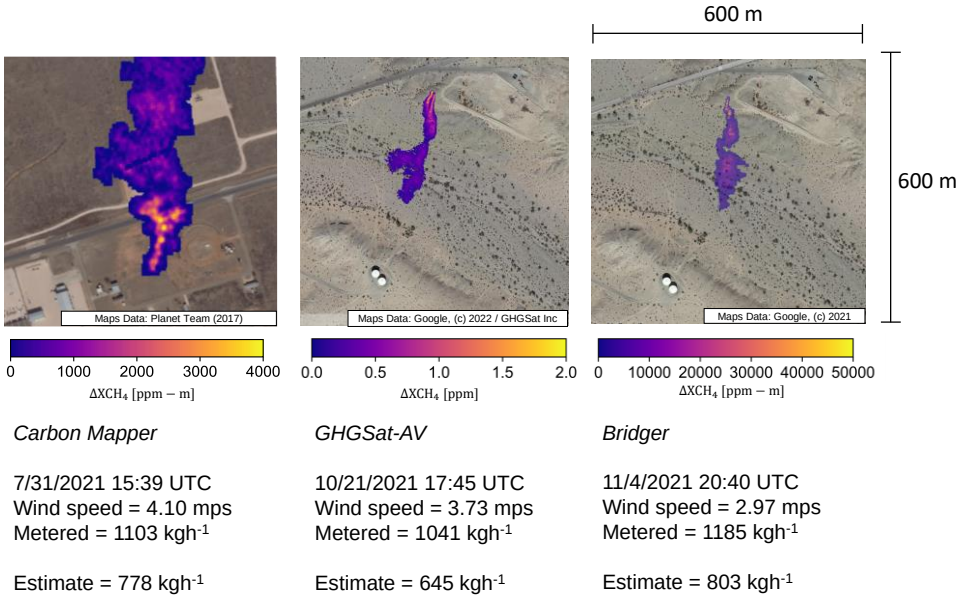

Figure 1: Examples of plume imagery for participating teams of CH_4 releases in the 1000 kg h^{-1} CH_4 range (1041-1185). Teams were allowed to report plume imagery in the color scale and metric of their choosing (A consistent color scale is not possible at reasonable image quality given differences in spectrometer specifications, **Table S1**). Metered release rate is reported as a 60 second rolling average and wind speed is reported as a 5 minute rolling average. Background imagery is from Google Earth (GHGSat-AV and Bridger) and Planet Team [30] (Carbon Mapper).

Over the course of the 10 testing days, 551 data points were generated for the three technologies tested in this paper. Here, a single data point describes an overpass, where a technology flew over top of the release stack (where Stanford was either releasing a non-zero CH_4 volume or a zero negative control) and the overpass was reported by Stanford. Across the three technologies, 472 data points are non-zero releases (85.6% of total), and 53 data points were intentional non-releases (zero volume negative controls, 9.6% of total). 26 data points (4.7% of total) were excluded by Stanford for insufficient plume development time and other reasons describing in Rutherford et al. [28]. The total sample sizes, not including data excluded by Stanford, are 114, 227, and 210, respectively for the Bridger, Carbon Mapper, and GHGSat-AV technologies.

Classification results for Bridger, Carbon Mapper, and GHGSat-AV are summarized in **Table 1**.

Table 1: Summary of overpass classification for controlled release participants. Results are organized by participant and data unblinding stage. Stage 1 corresponds to fully-blinded wind and release volume, stage 2 corresponds to unblinded 10-meter wind measurements, and stage 3 corresponds to half-unblinded release volumes. "Filtered: acquisition" indicates spectral data were not collected due to irregular plane trajectory or the plume being outside the field of view. "Filtered: algorithm" indicates that the algorithm was not able to produce an estimate of the presence or absence of methane based on the collected spectral data. "Missing data" refers to measurements for which the team did not submit data. Stanford excluded data points in which the emission rate was not held long enough to establish a consistent plume, or if the emission rate was not sufficiently steady during the release.

	Bridger			Carbon Mapper GAO			GHGSat-AV		
	1	2	3	1	2*	3*	1	2	3
Non-zero releases									
True positive	110	110	110	153	153	150	149	149	149
False negative	-	-	-	10	-	-	20	20	20
Filtered: acquisition	-	-	-	-	-	-	5	5	5
Filtered: algorithm	-	-	-	17	-	-	-	-	-
Missing data	-	-	-	-	-	-	8	8	8
Zero releases									
True negative	4	4	4	30	-	-	17	17	17
False positive	-	-	-	-	-	-			
Filtered: acquisition	-	-	-	-	-	-	1	1	1
Filtered: algorithm	-	-	-	-	-	-			
Missing data	-	-	-	-	-	-	1	1	1
Stanford exclusion									
Not established	-	-	-	16	15	15	9	9	9
Not steady	-	-	-	1	1	1	-	-	-

* Indicates that the full dataset was not submitted for Stages 2 and 3. In these cases Carbon Mapper submitted only true positive detections. Thus, "Not established" and "Not steady" counts may also be smaller due to Carbon Mapper filtering

Of the 114 overpasses by Bridger, none are excluded due to technical issues (see further details of data exclusion criteria in Rutherford et al. [28]). Minimum and maximum non-zero flow rates delivered to Bridger were 3.9 (3.9-4.0, 95% CI) and 1,426.7 (1,349.6-1,506.1) kg h^{-1} CH_4, respectively. Bridger detected all non-zero releases (110) and correctly classified all three negative controls as zero (i.e., there were no false negatives or false positives). We only dedicated a small number (11 or 10%) of releases < 100 kg h^{-1} CH_4 as this size range was covered in a separate publication by a partner research group [23]. No data points were excluded by Bridger due to quality control issues.

Of the 227 overpasses by Carbon Mapper, 17 data points are excluded on the Stanford side due to technical issues, including both insufficient plume development and unsteady release rate (see further details in Rutherford et al. [28]). Of the 210 overpasses with steady and established plumes, minimum and maximum non-zero flow rates delivered to Carbon Mapper were 9.8 (3.0-16.6, ±1 sigma) and 1,491 (1,439.9-1,549.0) kg h^{-1} CH_4, respectively. Carbon Mapper detected 85% of nonzero releases (153 of 180, with 27 false negatives or not estimated due to data processing issues) and correctly classified all negative controls as zero (30). False negatives were in the range 10.05-49.43 kg h^{-1} CH_4, and not estimated due to quality control issues were in the range 21.62-1088.11 kg h^{-1} CH_4. We dedicated 40 (22%) steady and established non-zero releases to small volumes < 100 kg h^{-1} CH_4, of which 21 (52.5%) Carbon Mapper detected. In these statistics, we include in the denominator 17 overpasses classified as quality control (QC) level 0 by Carbon Mapper.

Caution must be used in interpreting metered volumes < 50 kg h^{-1} CH_4 for Carbon Mapper trials. In Texas, the setup did not include a high accuracy Coriolis meter. Low flow rates were delivered with a Sierra Instruments QuadraTherm 640i insertion probe which has an uncertainty of +/- 170% (95% CI) at 10 kg h^{-1} CH_4 and +/-35% (95% CI) at 50 kg h^{-1} CH_4.

Of the 202 overpasses by GHGSat-AV, 9 data points are excluded on the Stanford side due to technical issues, including both insufficient plume development and unsteady release rate (see further details in Rutherford et al. [28]). Of the 193 overpasses with steady and established plumes, minimum and maximum non-zero flow rates delivered to GHGSat-AV were 5.0 (4.98 - 5.04, 95% CI) and 7,389.9 (6,991.6-7,804.0) kg h^{-1} CH_4, respectively. Note that because we were testing satellites simultaneously (although not GHGSat satellites), flow rates delivered to GHGSat-AV are substantially higher compared to those delivered to Carbon Mapper and Bridger. GHGSat-AV detected 86% of nonzero releases (149 of 174, with 33 false negatives, not estimated due to quality control issues, or not reported) and correctly classified 89% of negative controls (17 of 19, with 1 not estimated due to quality control and 1 not reported). We dedicated 50 (28%) steady and established non-zero releases to small flow rates < 100 kg h^{-1} CH_4, of which 27 (54%) GHGSat-AV detected. In these statistics, we include in the denominator 15 overpasses flagged by GHGSat-AV as quality control issues or not reported (see details of QC identification above).

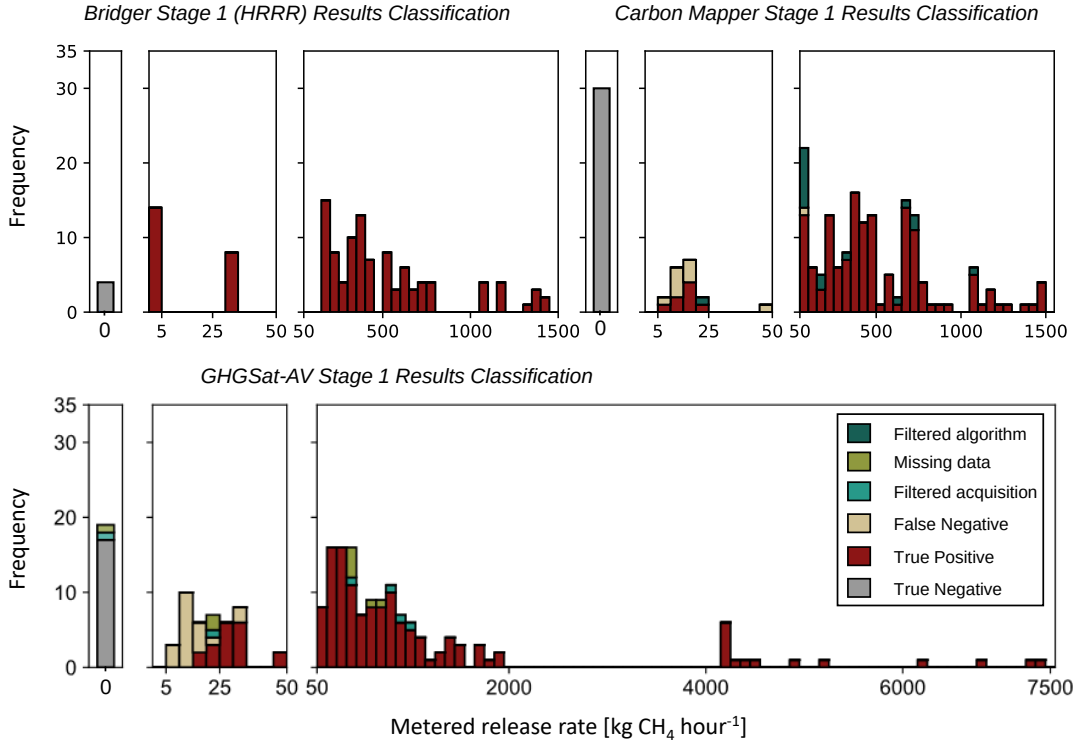

Figure 2: Histograms of overpass counts by metered release rate (kg CH_4 hr^{-1} averaged over 60 seconds, a conservative averaging period based on our 150 m plume establishment criteria and average wind speeds for all teams (around 3 m s^{-1})).) For each controlled release participant, we present (organized left to right): (i) negative controls (zero release), (ii) near-minimum detect release volumes (5 – 50 kg CH_4 hr^{-1}), and (iii) all other non-zero volumes (> 50 kg CH_4 hr^{-1}). Data are classified using the same scheme as in **Table 1**. Does not include data excluded by Stanford.

For the 110, 153, and 149 true positive (non-zero detections) estimates by Bridger, Carbon Mapper, and GHGSat-AV, respectively, we assess the quantification accuracy in **Figure 3** parity charts using ordinary least squares (OLS) regression, following the justification for OLS from Sherwin et al. [29]. In these plots, for the case of perfect quantification, the operator methane emission estimates would fall along the 1:1 line with no scatter. Quantification results are assessed for each round of the staged unblinding.

In Stage 1, the fully blinded stage, each team used the approach utilized in commercial operations. In commercial operations, in-situ wind data are usually not available, so operators must use modelled wind reanalysis products (based on temporally and spatially coarse atmospheric wind models). The first column in **Figure 3** shows results for Stage 1.

Bridger reported Stage 1 results using two different wind products, High Resolution Rapid Refresh (HRRR) and North American Mesoscale 12 km model (NAM12) (**Figure 3**). Performance is better for HRRR (slope = 1.06, R^2 = 0.78) than NAM12 (slope = 0.81, R^2 = 0.77). Bridger did

not submit uncertainty estimates so no vertical error bars are included. Carbon Mapper reported Stage 1 results using the HRRR wind product (slope = 0.33, R^2 = 0.35). Uncertainty estimates submitted are for 1-sigma error. Due to concurrent testing of satellite technologies (not including the GHGSat satellites), GHGSat-AV was tested across a much wider range of release rates (5 to >7,000 kg h^{-1}). For a consistent comparison across technologies, however, we restrict this linear fit to release rates < 2,000 kg h^{-1}. GHGSat-AV submitted results using the NASA Goddard Earth Observing System Forward Processing (NASA-GEOS FP) wind product (slope = 1.00, R^2 = 0.38). Error bars are for 1-sigma error. If we include all test release rates (5 to >7,000 kg h^{-1}), GHGSat-AV demonstrates a tendency to underestimate at higher flow rates (slope = 0.30, R^2 = 0.30, see **Figure S6**).

In Stage 2, teams were given the opportunity to resubmit estimates with unblinded in-situ 10-meter sonic anemometer wind speed and direction data (1 Hz resolution). For Bridger and GHGSat-AV, scatter in estimates decreased, with R^2 values rising to 0.92 and 0.78, respectively. For Carbon Mapper, R^2 did not increase in Stage 2 . The only case which saw improvement in the ordinary least squares slope term after being given wind data was GHGSat-AV, when including the full range of release levels (**Figure S6**).

In Stage 3, teams were given the opportunity to resubmit estimates after seeing true values for half of the release volumes (see description of our approach for partitioning volumes released in Supplementary Note 2). Across participants, the improvement in Stage 3 was mixed. For Bridger, there was no improvement in scatter between Stages 2 and 3, and only minor improvement in the slope term. For Carbon Mapper, there was slight improvement in scatter and the slope term between Stages 2 and 3. For GHGSat-AV, there was no improvement in variance between Stages 2 and 3, and only minor improvement in the slope term.

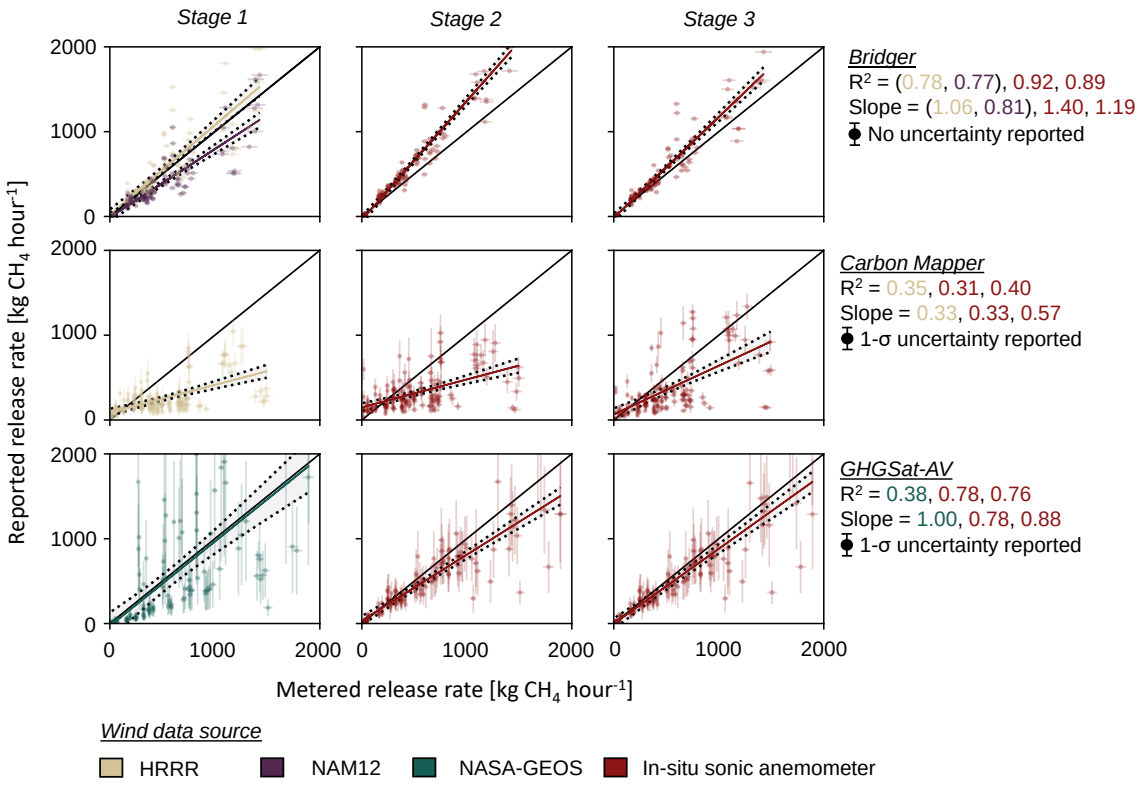

Figure 3: Parity charts of metered non-zero release rates (kg CH_4 hr^{-1} averaged over 60 seconds, a conservative averaging period based on our 150 m plume establishment criteria and average wind speeds for all teams (around 3 m s^{-1}) and reported participant estimates (including only data classified as true positive). Parity charts are organized by participant (rows) and unblinding stage (columns). Note that volumes > 2,000 kg CH_4 hr^{-1} were tested for GHGSat-AV, but for consistency with other operators were not included in this plot (See **Figure S6**). Error bars indicate 95% confidence intervals for Bridger and 1-sigma for Carbon Mapper and GHGSat-AV. Note that uncharacteristically short Carbon Mapper flightlines likely introduced significant downward bias into quantification results.

Residuals for relative error appear stationary for Bridger and GHGSat-AV. For Carbon Mapper, there is a tendency to overestimate at lower release levels, and a tendency to underestimate at higher release levels. Absolute and relative residuals are shown in **Figure S5**. The mean of percent deviations for Bridger is 8.6% [-37.0% to 96.0%, 95% CI]. The mean of percent deviations for Carbon Mapper is -16.0% [-82.6% to 273.5%]. The mean of percent deviations for GHGSat-AV is -22.8% [-82.3% to 210.1%]. Note that confidence intervals in ordinary least squares linear regression assume homoskedasticity (constant error term across the range of values). However, across all technologies there is higher absolute error residuals at higher release rates (**Figure S5**).

Wind speed measurement is an important aspect of CH_4 quantification algorithms, and improved wind speed accuracy should reduce the scatter in estimated emission rates (**Figure 3**). It would

seem logical that there might be a relationship between wind speed magnitude and accuracy. However, visually there does not appear to be a relationship between wind speed (5 minute rolling average) and fractional quantification error, with the exception of Bridger (HRRR wind product), where error is highest at wind speeds between 2 and 3 meters per second (mps). There does, however, appear to be a trend in the range of error with respect to wind speed. Interquartile range (IQR) is generally higher at lower wind speeds (**Figure S2-S4**).

After unblinding, teams had the opportunity to analyze the release data internally. Carbon Mapper informed Stanford that shorter flight lines, relative to field operations, were used to boost sample size in the controlled release experiment. However, upon review of the data, Carbon Mapper learned that using shorter flight lines significantly affected performance. Carbon Mapper has since re-evaluated the results from these controlled releases due to the fact that short flight lines in this set of controlled releases, coupled to the retrieval algorithm being used, resulted in lower-than-expected estimated quantities. Ayasse et al. [31]make a strong case that the low bias observed in these results is due to the use of shorter-than-typical flight lines. This should be taken into consideration reviewing the results of this study. Further testing is required to understand the quantification performance of Carbon Mapper under more typical operating protocols.

Differences in scene conditions between the trials in Gardendale and Ehrenberg may affect measurement results [32], [33]. The trial in Gardendale was conducted in an industrial park with buildings in the close vicinity (within 100 m). At the Ehrenberg location, the closest buildings (apart from a co-located municipal solid waste transfer station with a small office) were over 400 m away. Painted commercial rooftops have been known to affect retrieval algorithms [32].

The topography was also different between the two locations. The Ehrenberg tests took place in a barren desert landscape with uneven, rocky terrain and nearby dunes, which may have created unstable wind patterns near the release stack. In contrast, the Midland releases took place in a cleared field, with flatter terrain, although it is difficult to say if this led to more stable wind patterns due to the closer proximity of buildings.

The Gardendale releases took place in an active oil and gas basin, increasing the likelihood of confounding sources. On July 29, Carbon Mapper alerted Stanford of a large (variable, but estimated at over 1 tonne CH_4 per hour) unlit flare venting approximately 1000 m East of the controlled release site. Given that Carbon Mapper's quantification algorithm is applied a maximum of 150 m from the release origin, this is unlikely to significantly affect results.

This study demonstrates the performance of airplane-based remote-sensing technologies with an engineered point source emitter at a known location. Real-world emission surveys differ in several ways, with detection and quantification of sometimes intermittent sources with varying gas composition in unknown locations. If the underlying source is less consistent than our releases, that makes quantification harder, but is not a limitation of the technology or our testing. Bell et al. [23] tested quantification performance of Bridger with a source of varying gas composition and identified very little deterioration in methane quantification with gas mixtures including non-methane gas species.

Distinguishing between the quantification performance at high flow rates of point-source emitters and detection abilities near the minimum detection limit is important in assessing the limitations of our study. We do not expect quantification performance with an unknown source location to differ significantly from the results of this study. Especially at high flow rates, above the minimum detection limit, detection becomes trivial and the same quantification algorithm is applied regardless of source location. However, unknown location is a larger issue for testing of minimum detection limit. For example, between the Ravikumar et al. [34] single-blind testing of ground-based OGI cameras, in which release location was given, and Zimmerle et al. [35], who tested with no guidance on release location, there was an order of magnitude difference in minimum detection limit.

Perhaps the most accurate test of operational performance for airplane-based remote sensing was by Johnson et al. [21], in a fully-blinded design where Bridger was unaware even that they were being tested. However, this testing did not include high flow rate releases (all < 4 kg h^{-1} CH_4). Results of Johnson et al. also suggest a minimum detection limit of ~2 kg h^{-1} CH_4 (at 3 m s^{-1} wind speed), lower than the smallest release delivered to Bridger in this study.

In this study, we present an evaluation of three aircraft-based remote-sensing instruments. Recent work has demonstrated the widespread presence of large point-source emitters, which are unaccounted for in current official inventories and for which these aircraft-based instruments are uniquely suited to detect. In a recent study, Tyner and Johnson [36] construct modified provincial O&G CH_4 inventories, one based on aerial measurements and a separate inventory based on OGI surveys only. Their findings suggest that the two methods may capture distinct parts of the emissions distribution, and sources captured predominantly by the aerial measurements (largely unlit flares and tanks) drive a revised inventory estimate over an order of magnitude greater than an OGI based inventory.

If aerial technologies are to serve a greater role in CH_4 mitigation and inventory development, then improving confidence in quantification performance is essential. As aircraft-based remote-sensing technologies mature and become more widely adopted, field testing must happen on a much larger scale. Future work should include (i) establishing clear protocols (e.g., [24]) for testing so more groups, both inside and outside research institutions, can test new technologies, (ii) understanding key drivers of uncertainty in quantification such as wind speed, geographic conditions (i.e., land cover), and other meteorological conditions, and (iii) providing guidance for how controlled release testing (and estimated biases of technologies) should be used in interpreting results of basin-wide O&G CH_4 surveys.

Acknowledgments
We acknowledge Walt Godsil, Merritt Norton, Tyler Farmer-Molin, Scott Miller, and Mike Brandon of Rawhide Leasing for providing indispensable operational, logistical, and planning support for the experiment. Dana Walker of Volta Fabrication engineered and built the release apparatus for the experiment. Clay Bell made significant contributions to development of the data processing code. ExxonMobil, particularly Felipe Javier Cardoso-Saldaña, provided thoughtful feedback. We received remote logistical support from participants Ryan Mattson, Brody Wright, Warren Shaw, Jason McKeever, and Hanford Deglint (GHGSat); Mike Thorpe

and Pete Roos (Bridger); and Dan Cusworth, Riley Duren, Alana Ayasse, Andrew Thorpe, and Joseph Heckler (Carbon Mapper).

Supplementary Information
Available within this document

Funding sources
This study was funded by ExxonMobil, the Stanford Strategic Energy Alliance, and the Stanford Natural Gas Initiative, an industry consortium that supports independent research at Stanford University.

References

[1] Q. Saunois, M., Stavert, A. R., Poulter, B., Bousquet, P., Canadell, J. G., Jackson, R. B., Raymond, P. A., Dlugokencky, E. J., Houweling, S., Patra, P. K., Ciais, P., Arora, V. K., Bastviken, D., Bergamaschi, P., Blake, D. R., Brailsford, G., Bruhwiler, L., "The Global Methane Budget 2000–2017," *Earth Syst. Sci. Data Discuss*, doi: https://doi.org/10.5194/essd-2019-128.

[2] D. Brandt, A.R., Heath, G., Cooley, "Predictive analytics for natural gas leak detection and mitigation," 2018.

[3] Y. Chen *et al.*, "Quantifying Regional Methane Emissions in the New Mexico Permian Basin with a Comprehensive Aerial Survey," *Cite This Environ. Sci. Technol*, vol. 2022, p. 4323, 2022, doi: 10.1021/acs.est.1c06458.

[4] T. Lauvaux *et al.*, "Global assessment of oil and gas methane ultra-emitters," *Science (80-.).*, vol. 375, no. 6580, Feb. 2022, doi: 10.1126/SCIENCE.ABJ4351/SUPPL_FILE/SCIENCE.ABJ4351_SM.PDF.

[5] D. H. Cusworth *et al.*, "Intermittency of Large Methane Emitters in the Permian Basin," *Environ. Sci. Technol. Lett.*, 2021, doi: 10.1021/acs.estlett.1c00173.

[6] I. Irakulis-Loitxate *et al.*, "Satellite-based survey of extreme methane emissions in the Permian basin," *Sci. Adv.*, vol. 7, no. 27, Jun. 2021, doi: 10.1126/SCIADV.ABF4507/SUPPL_FILE/ABF4507_SM.PDF.

[7] C. Frankenberg *et al.*, "Airborne methane remote measurements reveal heavy-tail flux distribution in Four Corners region," *Proc. Natl. Acad. Sci.*, vol. 113, no. 35, 2016, doi: 10.1073/pnas.1605617113.

[8] R. M. Duren *et al.*, "California's methane super-emitters," *Nature*, vol. 575, 2019, doi: 10.1038/s41586-019-1720-3.

[9] R. A. Alvarez *et al.*, "Assessment of methane emissions from the US oil and gas supply chain," *Science (80-.).*, p. eaar7204, 2018.

[10] A. P. Ravikumar *et al.*, "Repeated leak detection and repair surveys reduce methane emissions over scale of years," *Environ. Res. Lett.*, 2020, doi: 10.1088/1748-9326/ab6ae1.

[11] C. E. Kemp and A. P. Ravikumar, "New Technologies Can Cost Effectively Reduce Oil and Gas Methane Emissions, but Policies Will Require Careful Design to Establish Mitigation Equivalence," *Cite This Environ. Sci. Technol*, vol. 55, pp. 9140–9149, 2021, doi: 10.1021/acs.est.1c03071.

[12] J. S. Rutherford *et al.*, "Closing the methane gap in US oil and natural gas production emissions inventories," *Nat. Commun.*, vol. 12, no. 1, Dec. 2021, doi: 10.1038/S41467-021-25017-4.

[13] D. R. Lyon, R. A. Alvarez, D. Zavala-Araiza, A. R. Brandt, R. B. Jackson, and S. P. Hamburg, "Aerial Surveys of Elevated Hydrocarbon Emissions from Oil and Gas Production Sites," *Environ. Sci. Technol.*, 2016, doi: 10.1021/acs.est.6b00705.

[14] D. M. Tratt *et al.*, "Airborne visualization and quantification of discrete methane sources in the environment," *Remote Sens. Environ.*, vol. 154, no. 1, pp. 74–88, Nov. 2014, doi: 10.1016/j.rse.2014.08.011.

[15] S. Conley *et al.*, "Application of Gauss's theorem to quantify localized surface emissions from airborne measurements of wind and trace gases," *Atmos. Meas. Tech.*, vol. 10, no. 9, pp. 3345–3358, 2017, doi: 10.5194/amt-10-3345-2017.

[16] A. K. Thorpe *et al.*, "Mapping methane concentrations from a controlled release experiment using the next generation airborne visible/infrared imaging spectrometer (AVIRIS-NG)," *Remote Sens. Environ.*, vol. 179, pp. 104–115, 2016, doi: 10.1016/j.rse.2016.03.032.

[17] E. D. Sherwin, Y. Chen, A. P. Ravikumar, and A. R. Brandt, "Single-blind test of airplane-based hyperspectral methane detection via controlled releases," *Elementa*, vol. 9, no. 1, Mar. 2021, doi: 10.1525/elementa.2021.00063.

[18] A. P. Ravikumar *et al.*, "Single-blind inter-comparison of methane detection technologies – results from the Stanford/EDF Mobile Monitoring Challenge," *Elem. Sci. Anthr.*, vol. 7, Jan. 2019, doi: 10.1525/elementa.373.

[19] D. H. Cusworth *et al.*, "Strong methane point sources contribute a disproportionate fraction of total emissions across multiple basins in the U.S.," Feb. 2022, doi: 10.31223/X53P88.

[20] E. Sherwin *et al.*, "Quantifying oil and natural gas system emissions using one million aerial site measurements," doi: 10.21203/rs.3.rs-2406848/v1.

[21] M. R. Johnson, D. R. Tyner, and A. J. Szekeres, "Blinded evaluation of airborne methane source detection using Bridger Photonics LiDAR," *Remote Sens. Environ.*, vol. 259, Jun. 2021, doi: 10.1016/J.RSE.2021.112418.

[22] B. M. Conrad, D. R. Tyner, and M. R. Johnson, "Robust Probabilities of Detection and Quantification Uncertainty for Aerial Methane Detection: Examples for Three Airborne Technologies," Jun. 2022, doi: 10.31223/X5S05F.

[23] C. Bell, J. Rutherford, A. Brandt, E. Sherwin, T. Vaughn, and D. Zimmerle, "Single-blind determination of methane detection limits and quantification accuracy using aircraft-based LiDAR," *Elementa*, 2022, doi: 10.1525/elementa.2022.00080.

[24] (METEC) Methane Emissions Technology Evaluation Center, "Airplane and Satellite Detection. Appendix to: METEC Controlled Test Protocol, Survey Emission Detection and Quantification," 2022.

[25] W. Shaw, "Measuring Methane Emissions using Satellite and Airborne Instruments Toward a Tiered Observation System," in *EnviroTech 2019*, 2019, [Online]. Available: https://esaa.org/wp-content/uploads/2021/02/ET2019-Warren-Shaw.pdf.

[26] M. Hunter, D., Thorpe, "Gas Mapping LiDAR Aerial Verification Program Final Report," 2017. [Online]. Available: https://auprf.ptac.org/wp-content/uploads/2018/08/17-ARPC-03-Gas-Mapping-LiDAR-Report-180417v2.pdf.

[27] Bridger photonics, "Performance of Gas Mapping LiDAR™ for Quantification of Very High Methane Emission Rates," 2021. [Online]. Available: https://www.bridgerphotonics.com/sites/default/files/inline-files/BridgerPhotonics_HighControlledReleaseRates.pdf.

[28] A. R. Rutherford, J., Sherwin, E., Brandt, "Documentation of experimental setup for 2021 Stanford field testing," 2022. [Online]. Available: https://eao.stanford.edu/sites/g/files/sbiybj22256/files/media/file/Method_description_Setup_and_Uncertainty_v18.pdf.

[29] E. D. Sherwin *et al.*, "Single-blind validation of space-based point-source methane emissions detection and quantification," Jul. 2022, doi: 10.31223/X5DH09.

[30] Planet Team, "Planet Application Program Interface: In Space for Life on Earth." San Francisco, 2017,

[Online]. Available: https://api.planet.com/.

[31] A. Ayasse, D. Cusworth, K. O'neill, A. Thorpe, R. Duren, and C. Mapper, "Performance and sensitivity of column-wise and pixel-wise methane retrievals for imaging spectrometers," Feb. 2023, doi: 10.31223/X5C95T.

[32] A. K. Ayasse *et al.*, "Evaluating the effects of surface properties on methane retrievals using a synthetic airborne visible/infrared imaging spectrometer next generation (AVIRIS-NG) image," *Remote Sens. Environ.*, vol. 215, pp. 386–397, Sep. 2018, doi: 10.1016/J.RSE.2018.06.018.

[33] M. Zhang, I. Leifer, and C. Hu, "remote sensing Challenges in Methane Column Retrievals from AVIRIS-NG Imagery over Spectrally Cluttered Surfaces: A Sensitivity Analysis," doi: 10.3390/rs9080835.

[34] A. P. Ravikumar, J. Wang, M. Mcguire, C. S. Bell, D. Zimmerle, and A. R. Brandt, "'Good versus Good Enough?' Empirical Tests of Methane Leak Detection Sensitivity of a Commercial Infrared Camera," *Environ. Sci. Technol*, vol. 52, p. 22, 2018, doi: 10.1021/acs.est.7b04945.

[35] D. Zimmerle, T. Vaughn, C. Bell, K. Bennett, P. Deshmukh, and E. Thoma, "Detection Limits of Optical Gas Imaging for Natural Gas Leak Detection in Realistic Controlled Conditions," *Cite This Environ. Sci. Technol*, vol. 54, pp. 11506–11514, 2020, doi: 10.1021/acs.est.0c01285.

[36] D. R. Tyner and M. R. Johnson, "Where the Methane Is - Insights from Novel Airborne LiDAR Measurements Combined with Ground Survey Data," *Environ. Sci. Technol.*, vol. 55, no. 14, pp. 9773–9783, Jul. 2021, doi: 10.1021/ACS.EST.1C01572/ASSET/IMAGES/LARGE/ES1C01572_0009.JPEG.

[37] S. Jongaramrungruang, G. Matheou, A. K. Thorpe, Z. C. Zeng, and C. Frankenberg, "Remote sensing of methane plumes: Instrument tradeoff analysis for detecting and quantifying local sources at global scale," *Atmos. Meas. Tech.*, vol. 14, no. 12, pp. 7999–8017, Dec. 2021, doi: 10.5194/AMT-14-7999-2021.

Supplementary note 1: Technologies tested

The three technologies tested in the controlled release experiments are briefly discussed in the main text. Carbon Mapper's Global Airborne Observatory and GHGSat's GHGSat-AV are hyperspectral imaging sensors which measure backscattered sunlight from Earth's surface and Bridger's GML is a hyperspectral sensor (based on wavelength modulated spectroscopy technology) which measures backscattered light from an active laser. In Table S1 we summarize the key parameters used to describe hyperspectral sensors. The fitting window and spectral resolution describe the range of wavelengths measured by the spectrometer and the width of the bands (or channels). According to Jongaramrungruang [37], a sufficiently refined spectral resolution is important to minimize "spectral artifacts" picked up by the spectrometer but not related to CH4. However, signal-to-noise ratio deteriorates at higher spectral resolution (as fewer photons are counted at each pixel [37]). Spatial resolution is related to the instantaneous field of view (FOV), which describes the angle subtended by a single pixel. The finer the spatial resolution, the more accurately remote sensing technologies will be able to attribute methane plumes to specific operations or equipment. Field of view and swath width describe the angle and width covered in a single flight pass.

Table S1: Summary of sensor parameters for all operators:

Sensor/Organization	Fitting window [nm] (Spectral resolution)[5]	instantaneous FOV [degrees] (spatial resolution [m])[1,2]	FOV [degrees] (swath width [m])[1]	Signal-to-noise ratio[3,4]
GML/ Bridger	(2e-5)	0.03 (2)	32.5 (120)	
GAO/ Carbon Mapper	2100-2450 (5)	0.06 (3)	34 (2000)	>400
GHGSat-AV/ GHGSat	1660 - 1670 (0.3)	0.03 (1.5)	14 (750)	350

[1]At controlled release altitude
[2]Instantaneous FOV is defined as the angle subtended by a single pixel (or detector element)
[3]At 2300 nm methane band
[4]Bridger GML measurements are performed at 1651 nm. Bridger declined to share its signal-to-noise ratio
[5]Bridger does not use a fit to measure the path integrated concentration

Supplemental note 2: Round 3 release volume unblinding

For the second round of data unblinding (stage 3), participants were given the opportunity to generate methane estimates with half of the release dataset unblinded. Datasets were randomly partitioned into a half "training set" (sent to teams) and half "test set" (hold out). Here, datasets are split on the basis of unique volumes delivered, which doesn't necessarily correspond to 50% of timestamped overpasses since Stanford would hold a single volume for multiple overpasses. Further, stage 3 datasets were delivered to teams prior to Stanford analysis of data exclusion, thus some of the unblinded data corresponds to non-established plumes.

Table S2: Summary of overpass classification for controlled release participants and data unblinded for Stage 3 only. Results are organized by participant and data unblinding stage

	Bridger	Carbon Mapper GAO	GHGSat-AV
Non-zero releases			
True positive	59	77	61
False negative		4	11
Filtered acquisition			2
Filtered algorithm		11	
Missing data			4
Stanford exclusion			
Not established		6	3
Not steady		0	

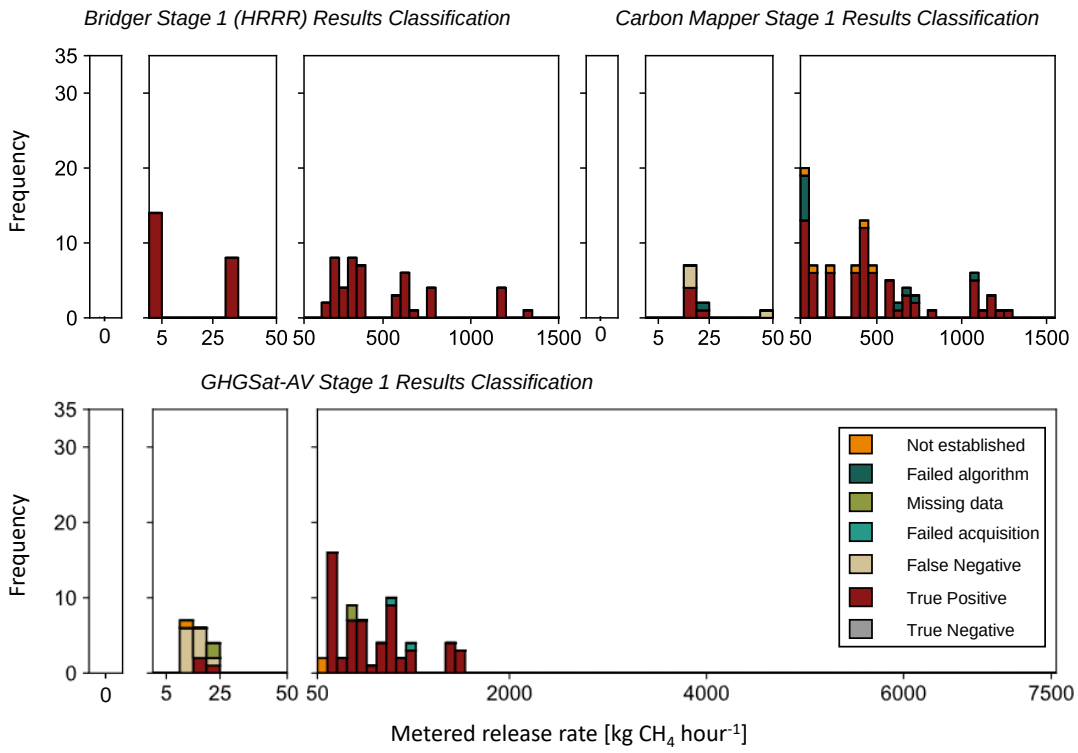

Figure S1: Histograms of overpass counts by metered release rate for only data unblinded to teams for the Stage 3 unblinding (metered release rates were shared for roughly half the data).

Supplemental note 3: Supporting tables and figures

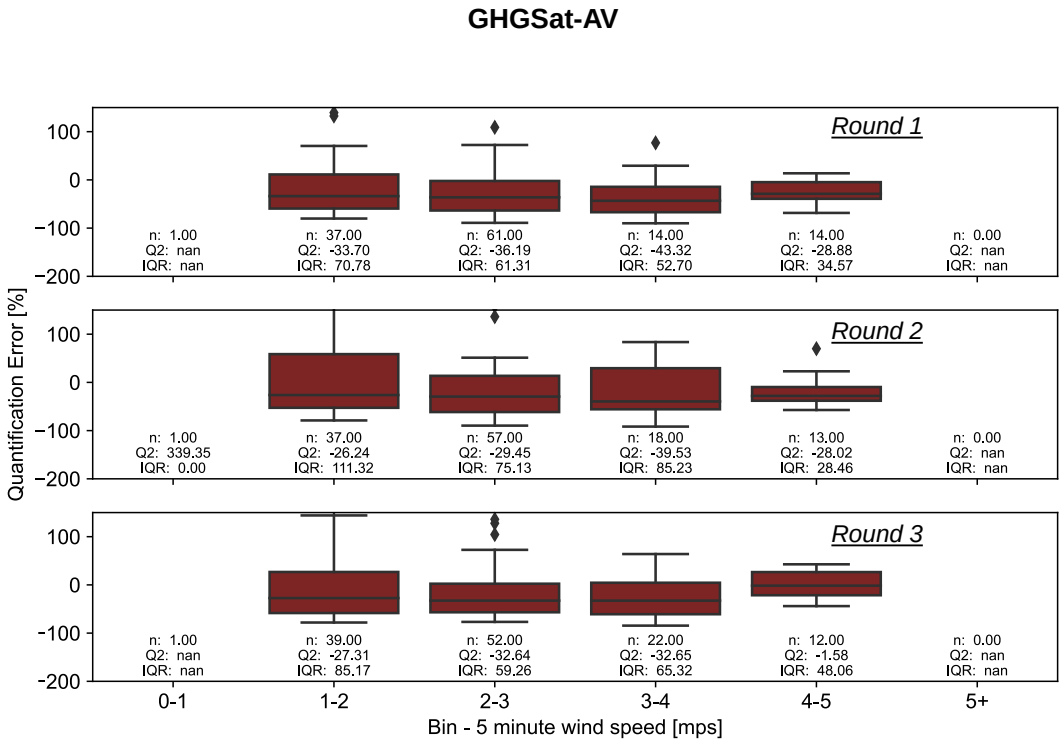

Figure S2: Box and whisker plot of quantification error (percent difference between GHGSat-AV reported estimate and the actual release rate, 60 second mean, kg CH_4 hr^{-1}) binned by 5 minute average wind speed at 10 meters. Box and whisker plot illustrates the median (solid line), inner quartiles (box), and 95% confidence interval (whiskers).

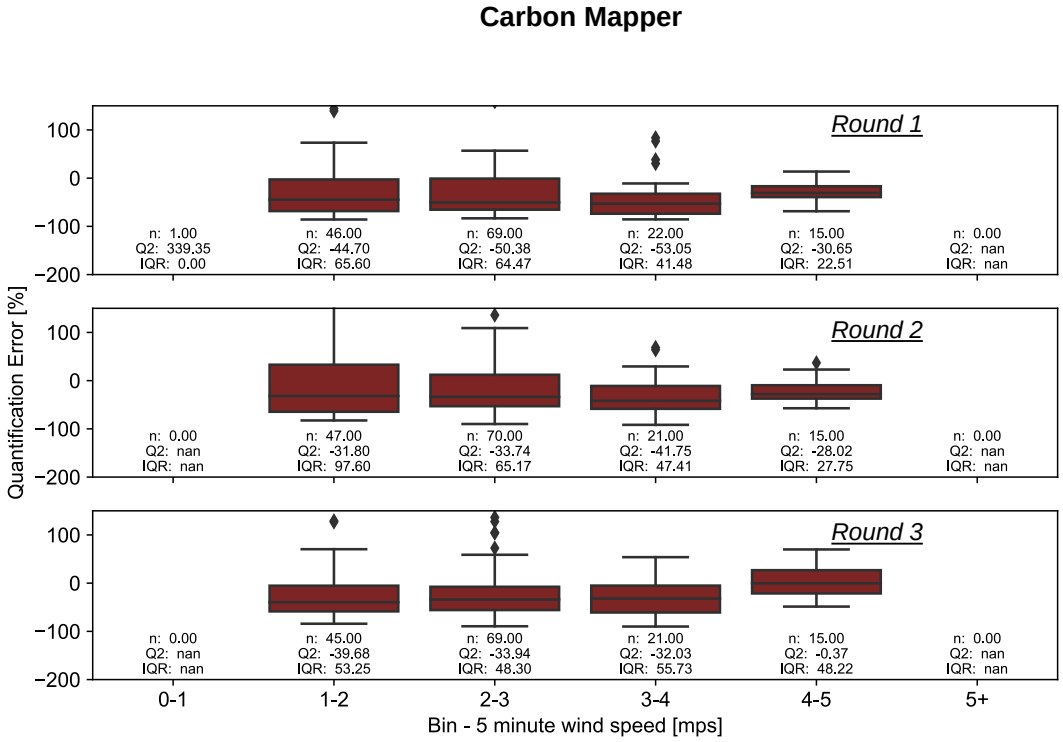

Figure S3: Box and whisker plot of quantification error (percent difference between Carbon Mapper reported estimate and the actual release rate, 60 second mean, kg CH_4 hr^{-1}) binned by 5 minute average wind speed at 10 meters. Box and whisker plot illustrates the median (solid line), inner quartiles (box), and 95% confidence interval (whiskers).

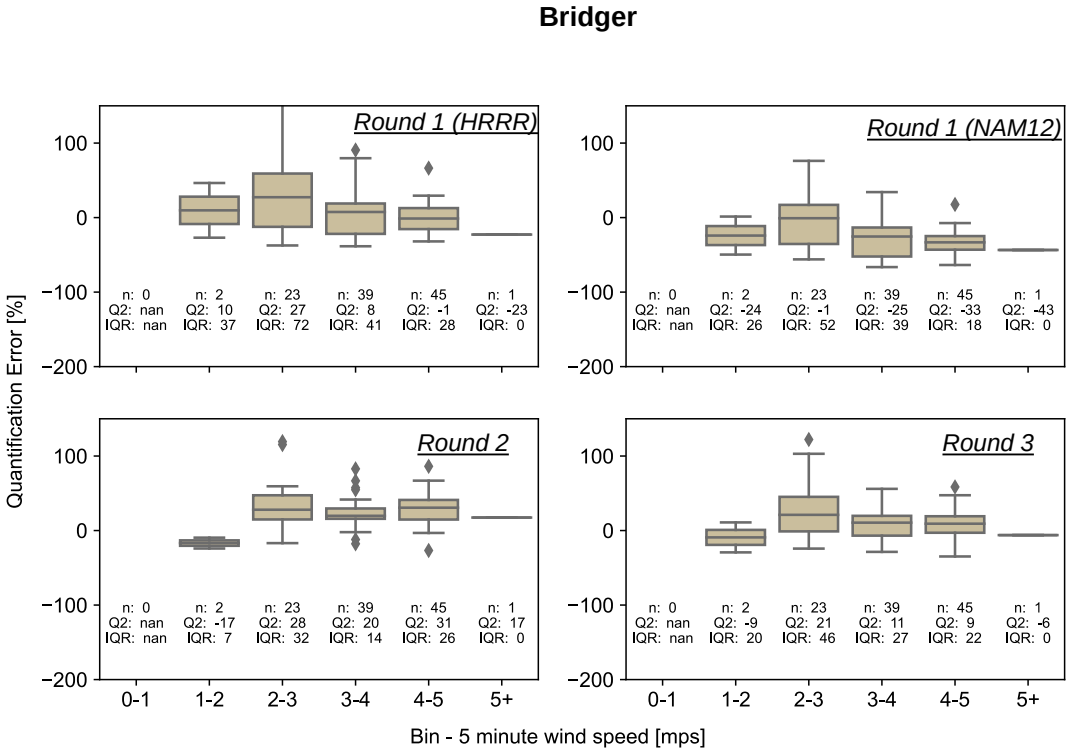

Figure S4: Box and whisker plot of quantification error (percent difference between Bridger reported estimate and the actual release rate, 60 second mean, kg CH_4 hr^{-1}) binned by 5 minute average wind speed at 10 meters. Box and whisker plot illustrates the median (solid line), inner quartiles (box), and 95% confidence interval (whiskers).

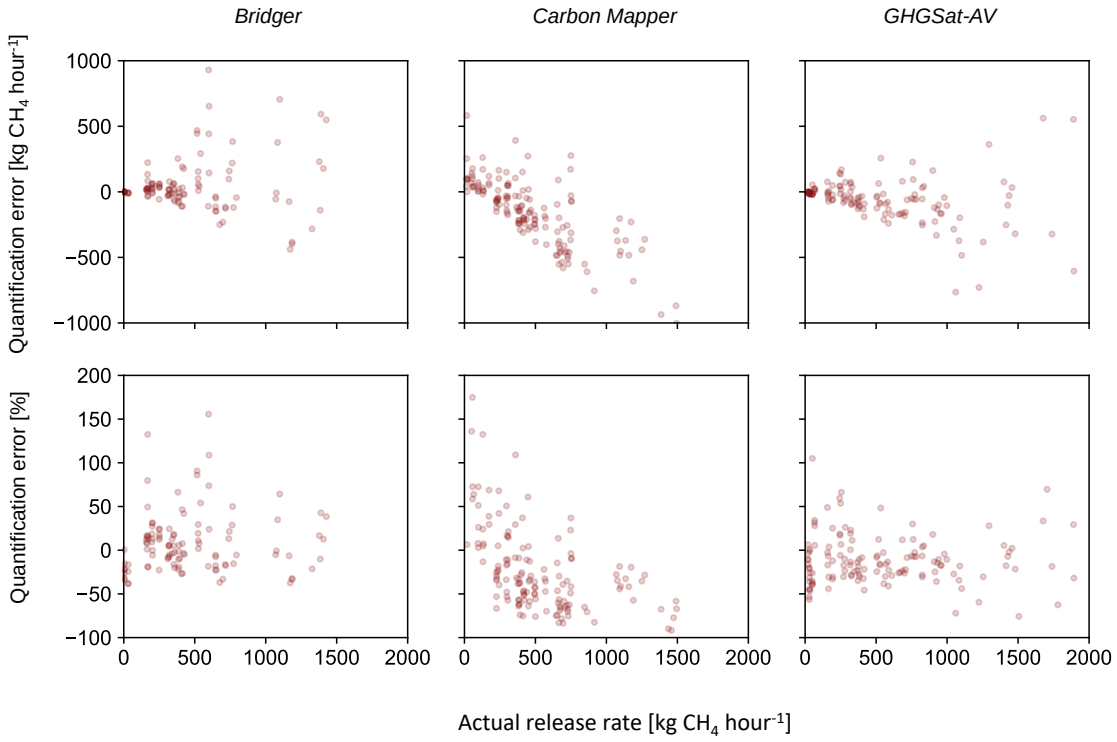

Figure S5: Quantification error magnitude (top row) and percent (bottom row) by operator.

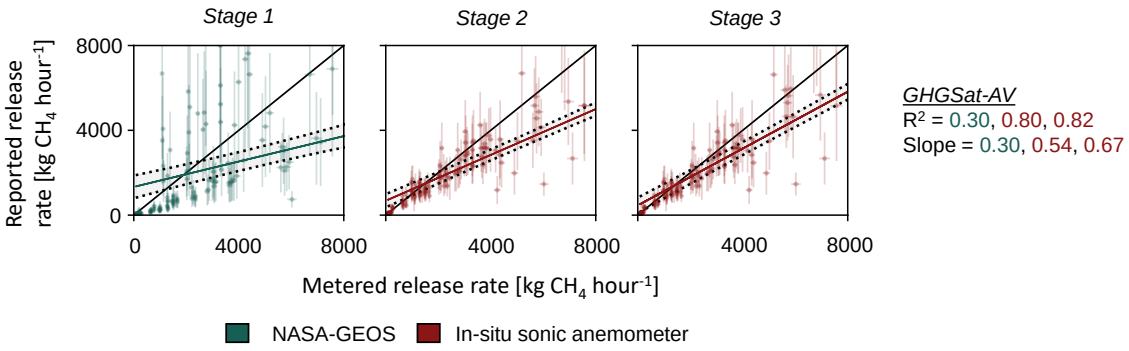

Figure S6: Parity charts for GHGSat-AV of metered non-zero release rates (kg CH4 hr-1 averaged over 60 seconds, a conservative averaging period based on our 150 m plume establishment criteria and average wind speeds for all teams (around 3 m s-1).) and estimates (including only data classified as true positive) including volumes > 2,000 kg CH4 hr-1. Note that for consistency volumes > 2,000 kg CH4 hr-1 were not included in the main text plot (See Figure 3). Error bars indicate 95% confidence intervals.

Table S3: Daily experimental summaries

Date	Operator tested	Start time [Local, (UTC)]	Experiment duration [hours]	Overpasses [#]	Average revisit time [minutes]	Flight altitude, average [feet above ground level][1,2]	Average wind speed [m s^{-1}]
30-Jul-21	Carbon Mapper	10:27 (15:27)	2.4	68	2.1	9,133	2.3
31-Jul-21	Carbon Mapper	10:22 (15:22)	0.6	17	2.0	9,180	2.9
3-Aug-21	Carbon Mapper	10:22 (15:22)	4.7	139	2.0	9,178	3.9
18-Oct-21	GHGSat-AV	10:14 (17:14)	2.0	35	3.4	10,010	8.8
19-Oct-21	GHGSat-AV	10:46 (17:46)	2.9	40	4.3	9,941	2.8
20-Oct-21	GHGSat-AV	10:44 (17:44)	3.0	41	4.4	9,935	3.3
21-Oct-21	GHGSat-AV	10:43 (17:43)	3.0	45	4.0	6,572	3.7
22-Oct-21	GHGSat-AV	10:50 (17:50)	3.1	43	4.3	9,930	2.0
3-Nov-21	Bridger	10:42 (17:42)	3.7	56	4.0	688	3.3
4-Nov-21	Bridger	10:00 (17:00)	3.9	56	4.1	693	3.3

[1]Ground level at the release stack in Ehrenberg is approximately 344 feet above sea level. Ground level at the release stack in Gardendale is approximately 2917 feet above sea level.

[2]Carbon Mapper and GHGSat-AV altitude estimates are based upon FlightRadar24. Bridger altitude is based on measurements from Bridger's own GML LiDAR. Note that the Bridger GML LiDAR altitude measurements are 44% higher compared to FlightRadar24 estimates (477 ft and 481 ft agl for November 3 and 4, respectively).

Table S4: Specifications of Quadratherm flow meters used in experiments

Pipe #	Size	Internal Diameter (inches)	Area [ft2]	Full scale flow rate, 162928/ 218645 [scfh]	Full scale flow rate, 308188 [scfh]	Gas setting[1]
Texas campaign						
1	2" SCH10	2.163	0.026	30,621	24,247	Methane
2	4" SCH40	4.026	0.088	106,086	84,004	Methane
Arizona campaign						
1	2" SCH40	2.067	0.023	27,963	22,143	aMethane
2	4" SCH40	4.026	0.088	106,086	84,004	aMethane
3	8" SCH40	7.981	0.347	416,892	330,116	aMethane
4	0.5" SCH40	0.62	0.002	-	-	-

[1]"Methane" refers to air QuadraTherm calibration settings, and "aMethane" refers to actual gas QuadraTherm calibration settings. See further discussion of these calibration settings and implication for error in Rutherford et al. [28] section 4.3.

Table S5: Staged unblinding schedule

Operator	Submitted Round 1	Received wind data	Submitted Round 2	Received half unblinded volumes	Submitted Round 3
Carbon Mapper	28-Oct-21	12-Jan-22	14-Jan-22	25-Jan-22	28-Feb-22
GHGSat-AV	16-Nov-21	8-Dec-21	28-Jan-22	8-Feb-22	24-Feb-22
Bridger	17-Nov-21	8-Dec-21	20-Dec-21	1-Feb-22	28-Feb-22

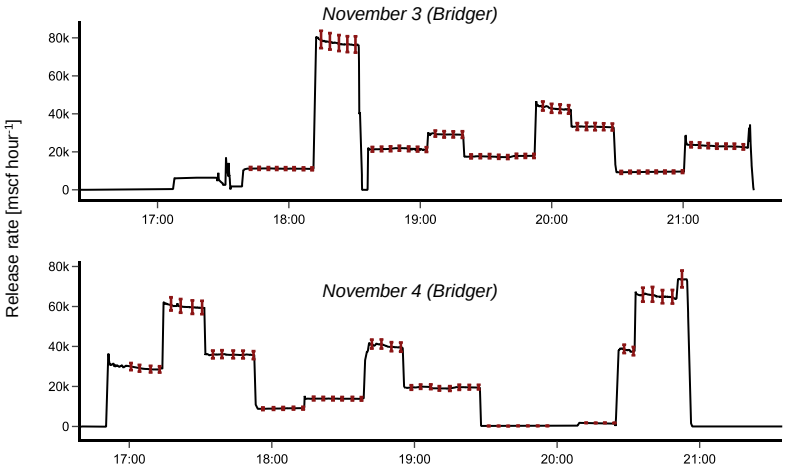

Figure S7: Release rate time series for Bridger

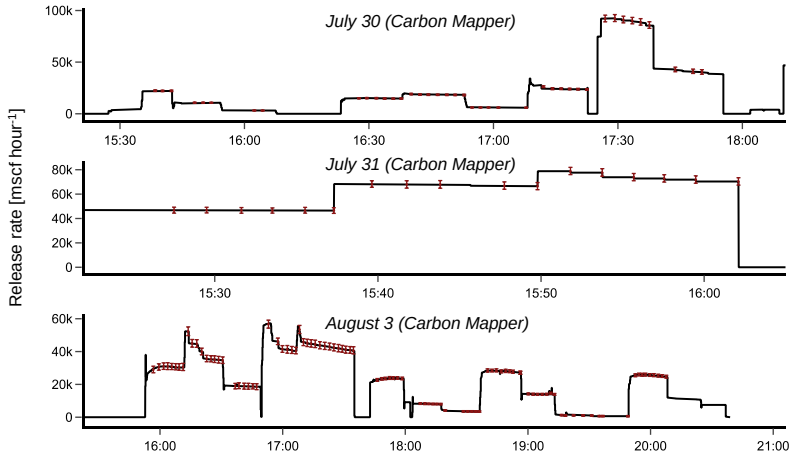

Figure S8: Release rate time series for Carbon Mapper

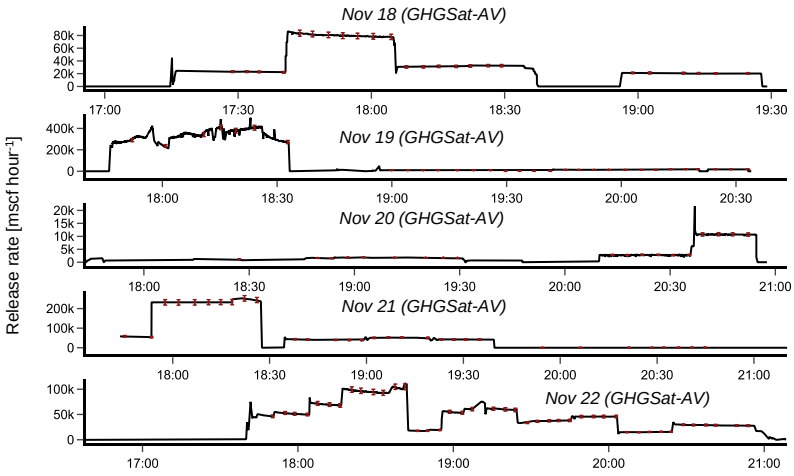

Figure S9: Release rate time series for GHGSat-AV

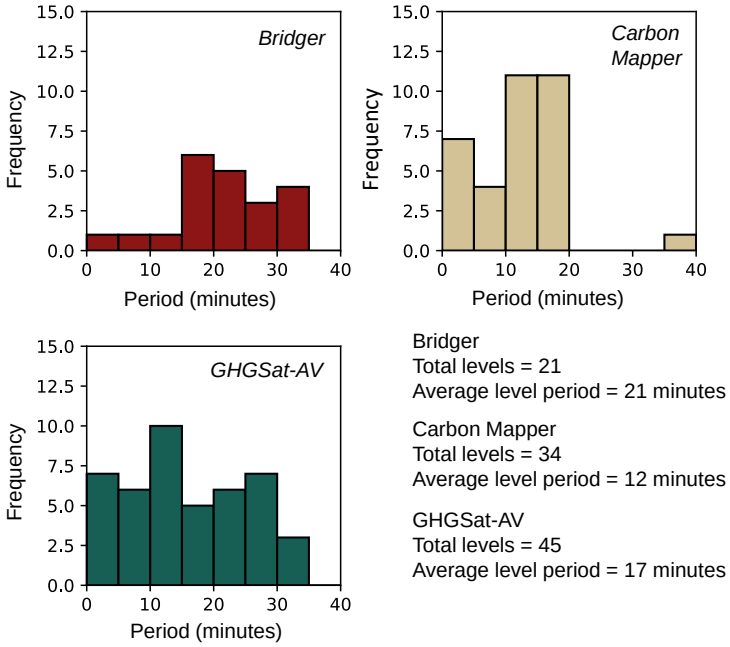

Figure S10: Histogram of level periods for all operators (span of time that a release rate was held before changing to a different release rate). Bins represent emissions with duration between the minimum and maximum bin x-value.